

Spreading of a Multicomponent Drop in Water: Solutions and Suspensions

Andrey Y. Ilinykh*

Ishlinsky Institute for Problems in Mechanics of the Russian Academy of Sciences, Moscow, 119526, Russia

*Corresponding Author: Andrey Y. Ilinykh. Email: ilynykh@ipmnet.ru

Received: 31 October 2019; Accepted: 13 March 2020

Abstract: The distribution of material resulting from the impact of a freely falling drop with a target liquid has been studied by photo and video registration methods. Different cases have been investigated by considering drops made of aqueous solutions (ink, salt, acid) and including fine solid particles (i.e., suspensions). New features have been observed in terms of flow dynamics and thin components produced as a result of the impact (such as banded elements, ligaments, and vortices at the surface of the liquid). In particular, the characteristics of emerging netlike structures have been found to depend on the size of the suspension clusters. For the case of acetic acid, a different patterning behavior has been obtained: sequences of concentric arcs are produced in that case. However, linear scaling laws and the discrete nature of the distribution of the droplet material seem to be features common to all the cases considered.

Keywords: Drop impact; splashes; ligaments; material distribution

1 Introduction

The processes initiated by the drop immersing into a fluid or by their collision with a solid surface are of interest due to the wide spreading of the phenomenon in nature and modern technologies. The element classification of flow patterns including a submerging drop, ejected splashes, a crown with an edge chevron, a relatively thick cumulative jet and a thin streamer, groups of capillary waves were presented by Worthington [1]. The question posed in his works on the nature of the formation and the magnitude of the flow velocity in the region of the falling drop still remains unanswered. The depending on impact regimes on Weber and Froude numbers was found experimentally later [2].

The informational content of flow patterns increased as lighting and photographic techniques improved. With increasing light sources brightness and the resolution of the photographic technique, the details of the structure at all evolution phases of flows of drop immersion became resolvable [3].

In later studies, the frequency spectrum of probing electromagnetic radiation was significantly expanded, and traditional illuminators in the optical range were supplemented by X-ray sources [4]. The thickness of the primary departing sheet was determined by means of short-wave radiation and did not exceed 0.1 mm in the case of silicone oil droplet immersing in silicone oil. Using high-resolution recording equipment, it was established that the primary ejecta sheet can be flat and twisted depending on the type of fluid [4]. Liquid inks were added to the drop fluid for visualization of the drop material



This work is licensed under a Creative Commons Attribution 4.0 International License, which permits unrestricted use, distribution, and reproduction in any medium, provided the original work is properly cited.

transfer in the flow pattern. Modern technologies enable to resolve drop splash patterns with pixel resolution up to $1.04 \mu\text{m px}^{-1}$ and frame rates up to 5 million fps [5].

The high spatio-temporal resolution of the equipment enabled to identify the azimuthal instabilities in the spot of contact between the drop and the target-fluid at the early stages of immersion already ($\sim 10 \mu\text{s}$). The instabilities are transformed into vortex structures in a short period of time (up to $30 \mu\text{s}$ from the moment of contact), which are of two counter-rotating streamwise vortices being about the edge of ejecta sheet connecting both liquids (double layer). It was shown that the structure of azimuthal instabilities depends of the difference in densities or surface tension coefficients of the fluids. The difference of densities leads to the appearance of ring structures (by analogy with the drop falling on a solid surface), and the difference between the surface tension coefficients increases the intensity of the observed effect [5].

The task of drop impact includes wide range of conditions with a wide set of flow components. In the case of impact with a solid surface, drop fluid propagates with producing a number of fundamental fingers rapidly expanding along the surface from a spot of the primary contact. The number of fingers depends on the inertial-viscous interaction [6] and remains approximately constant during the expansion [7].

At impact with wet solid surface or thin fluid film on it cylindrical sheet and a number of secondary droplets are generated with the diameter depending on the fluid properties and kinematic parameters, splashing-boundary regime depending on Reynolds and Ohnesorge numbers [8], the number of jets increasing with Weber number [9]. Capillary waves on the sheet were measured experimentally and calculated analytically, mechanism of crown formation with capillary waves and a cloud of secondary droplets ejected by the capillary breakup of the streams was considered at [10]. The investigations of interactions of droplets and solid surfaces get an important role since this process wide spreads in technical applications (cooling by fluid jets and films [11], printing, waterjet cutting, dip-pen nanolithography [12]). The unsteady internal flow of evaporating droplets under high-temperature environment is of special interest for cooling processes [13].

Separation, selection and different mechanisms of manipulation of separated water and oil droplets by the fluidic oscillator in the biochemical application were observed [14]. Droplet motion in an electric field is of specific interest. Flow patterns in different regions of the circulation-deformation map for a liquid drop being in the electric field were studied [15].

After pinching off the volume oscillations of drop remain for a long time. At the contact with target fluid small volume of air is involved in the fluid with producing bubbles of different classification [16]. At the drop impacts, a thin horizontal sheet of fluid (ejecta) is developing from the neck region of two fluids with ten times larger velocity than impact velocity of the drop [17]. An immersing drop forms a cavity in the target liquid, the shape and dynamics of which has been studied both numerically and experimentally in a large number of works [18,19], and a growing crown. Systems of annular capillary waves have been resolved on the surface of an immersed drop [20], on the side surfaces of the crown [21] and around it [22].

After filling the cavity and spreading the crown, the annular depression with complex geometry (socket) remains in the target-fluid surface, in the center of which a reverse jet gradually forms, both sufficiently thick (cumulative jet) and thin (streamer) with sequences of small droplets (spray) ejecting from the top. The nature of the flows depends on many parameters of the problem, and first of all, on the size of the drop and the contact velocity (or the height of falling). A classification of the observed flow regimes is given in [23].

In natural and technological processes, along with solutions, an important role is played by the impact of emulsions and suspensions. So, for example, raindrops passing through atmospheric layers collect solid suspended particles with different dispersion (dust, soot, metals). Drops of fog absorb harmful impurities, including ones from the most polluted layers of the atmosphere, which leads to a significant excess of the maximum permissible concentration of pollutants in the air. Drops flying into the atmosphere take out

organic substances and biomaterials, participate in the exchange of microbes and viruses and contribute to the spread of mass infections [24].

In industry, pure and fraught drops of water are used for ecological cleaning of surfaces. A simple criterion of the particle removal and influence of drop velocity and thickness of the fluid layer at the performance of cleaning and erosion were shown in [25]. Stabilization and destabilization of the interfacial properties of an emulsion are used in different applications. The general role in these properties plays drainage time that depends on the viscoelasticity of the matrix fluid (viscoelasticity reduces the drainage time) [26].

The aim of this paper is a high-resolution experimental study of flow patterns formed during the interaction of miscible and immiscible fluids (oil droplets in water) and suspensions, analysis of the effect of droplet composition on the dynamics of flows.

2 General Parameters of the Problem

The parameterization of fluid flows with a free surface and the planning of experiments are traditionally carried out on the basis of the system of fundamental equations and boundary conditions. The acoustic effects are neglected in this work; fluids are considered incompressible. Each of the fluids (a drop and a target-fluid) and the interface are characterized by their own sets of physical quantities, which include density (air ρ_a , drop liquid ρ_d and target-liquid ρ_t , further $\rho_{a,d,t}$), kinematical $\nu_{a,d,t}$ and dynamical $\mu_{a,d,t}$ viscosities, full $\sigma_d^a, \sigma_t^a, \sigma_t^d$ and density normalized $\gamma_d^a = \sigma_d^a/\rho_d, \gamma_t^a = \sigma_t^a/\rho_t, \gamma_t^d = \sigma_t^d/\rho_t$ cm³/c² surface tension coefficients at the droplet-air boundaries, target fluid-air, interface of immiscible droplet and target fluids, diffusion coefficients of the droplet material κ_t^d and marking admixtures κ_t^{md} in target-fluid, as well as temperature (considered equal for all the environments $T_d = T_t = T_a$). The values of the parameters for water and mineral oil are given in Tab. 1.

Table 1: Parameters of fluids

Liquid	Parameter			
	$\rho, \text{g} \times \text{cm}^{-3}$	$\sigma, \text{g} \times \text{c}^{-2}$	$\gamma, \text{cm}^3 \times \text{c}^{-2}$	$\mu, \text{g} \times \text{cm}^{-1} \times \text{c}^{-1}$
Water	1.00	73	73	0.01
Acetic acid (9%)	1.014	55	54.2	0.012
Copper sulfate water solution	1.206	74	62	0.02

Since the calculation of the dropping process taking into account physically reasonable equations and boundary conditions presents great difficulties, it is advisable to conduct a large-scale spatio-temporal analysis of the problem to determine the requirements for the experimental technique, in particular, to determine the characteristic length and time scales.

The physical parameters of the problem determine sets of time and length scales, which are divided into several groups. In one of them, the scales are set only by the physical parameters of the matter; in others, they include size or velocity of the drop.

The first group of linear scales includes the capillary-gravitational scale $\delta_g^\gamma = \sqrt{\gamma/g}$, contained in the dispersion equation of short surface waves, and dissipative-capillary scales $\delta_\gamma^v = v^2/\gamma, \delta_\gamma^k = \kappa^2/\gamma$, and $\delta_g^v = \sqrt[3]{v^2/g}$. One part of temporal scales includes environmental parameters, $\tau_g^\gamma = \sqrt[4]{\gamma/g^3}, \tau_\gamma^v = v^3/\gamma^2$, the other includes the size, $\tau_\gamma^d = \sqrt{D^3/\gamma}, \tau_\gamma^v = vD/\gamma$, and velocity of drop at the previous contact, $\tau_U^d = D/U_d, \tau_g^U = U_d/g$. For water, the largest and smallest length scales are $\delta_{\min} = \delta_\gamma^v = 1.37 \cdot 10^{-6}$ cm

and $\delta_{\max} = \delta_g^\gamma = 0.27$ cm, respectively, and time scales $\tau_{\min} = \tau_\gamma^v = 1.9 \cdot 10^{-10}$ s and $\tau_{\max} = \tau_\gamma^d = 3.2 \cdot 10^{-2}$ s. The largest scales are in the range of characteristic scales of processes on the fluid surface, in particular, the lengths and periods of capillary waves $\delta_g^\gamma = \sqrt{\gamma/g}$. The Smallest scale $\delta \sim 10^{-8}$ is within the range of intense atomic-molecular processes $\tau \sim 10^{-10}$ c ($\delta_\gamma^v, \tau_\gamma^v$).

Values of the characteristic scales were taken into account when developing the experimental technique (spatio-temporal resolution of the recording equipment) and choosing the size of the observation area, which should be sufficiently large and contain all the studied components of the studied flow. Relations of characteristic scales form a set of dimensionless combinations, including traditional numbers, such as Reynolds $Re_d = U_d D_d / \nu_d$, Froud $Fr_d = U_d^2 / g D_d$, Weber $We_d = U_d^2 D_d / \gamma_d$, Bond $Bo = g D^2 / \gamma_d^a$, Ohnesorge $Oh = \nu / \sqrt{\gamma D}$, and the capillary ratio $Ca_U^v = U_d / U_\gamma^v$. Typical values of the dimensionless parameters for the conditions of the experiments, which are given in Tab. 2, differ significantly from unity (with the exception of the Bond number), that complicates the interpretation of the results in the traditional dimensionless ratios.

Table 2: Dimensionless parameters of the experiment

Number	Fluid		
	Water	Acetic acid (9%)	Copper sulfate water solution
Re	10500	8000	5250
Wb	400	440	440
Fr	140	170	152
Bo	2.4	2.6	2.8
Oh	$18 \cdot 10^{-4}$	$26 \cdot 10^{-4}$	$39 \cdot 10^{-4}$
Ca_U	0.034	0.055	0.0008

Differences in the composition of the substance of the droplet and the target fluid allow us to characterize the ongoing processes with another group of combinations, including the following dimensionless relations:

- relative density difference of contacting media $R_\rho = (\rho_t - \rho_d) / (\rho_t + \rho_d)$ (Atwood number),
- surface tension coefficients $R_\sigma = (\sigma_t - \sigma_d) / (\sigma_t + \sigma_d)$,
- dynamic viscosities $R_\mu = (\mu_t - \mu_d) / (\mu_t + \mu_d)$.

In these experiments, the initial phase of contact and immersion of water droplets (clean, colored or loaded with coal dust of various dispersion) and oil in water was recorded.

Table 3: The values of the relative coefficients

Droplet material	Droplet diameter D_d , cm	Relativities		
		Density, R_ρ	Surface tension, R_σ	Viscosity, R_μ
Water	0.42	0	0	0
Acetic acid (9%)	0.38	-0.007	0.14	-0.09
Copper sulfate	0.42	-0.09	-0.007	-0.33

Drops with a diameter of $D_d = 0.3 \div 0.5$ cm freely fell in air from a height $H = 40 \div 80$ cm, the velocity at the moment of contact with the smooth surface of the target liquid was $U = 2 \div 3$ m/s (which corresponds to the formation of an expressed backward jet [23]).

3 Experimental Method

The experiments were performed on the TBP setup, part of the complex URF “HPC IPMech RAS,” a schematic image and photograph of which are shown in Fig. 1. The target liquid is placed in pool 1 with depth h_l (in the experiments we used glass pools with size of $30 \times 30 \times 5$ cm, square Petri dishes with size of $12 \times 12 \times 1.5$ cm or containers $16 \times 16 \times 8$ cm), over which drop dispenser 9 was installed at a height.

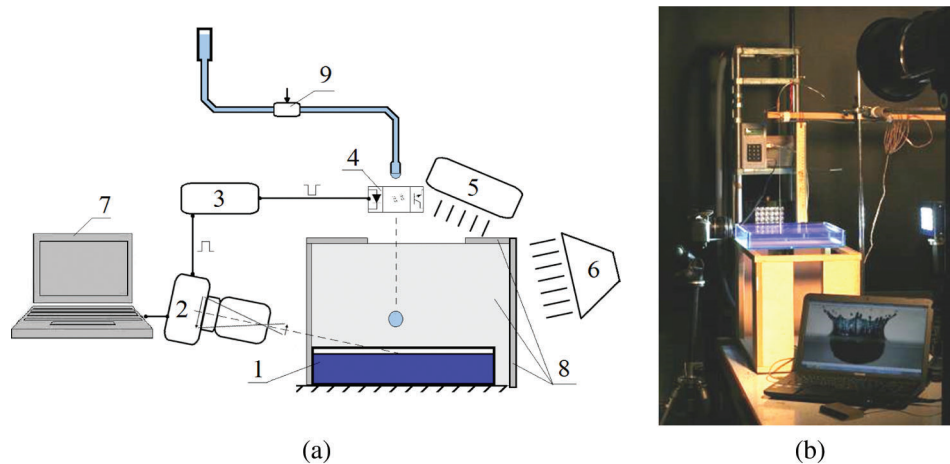


Figure 1: Experimental setup: a) – principal scheme of the setup (1 – reservoir, 2 – photo- or video camera, 3 – control block, 4 – droplet pinch off sensor, 5, 6 – light sources, 7 – computer, 8 – protective screens, 9 – dispenser; b) – photo of the setup

The observation area, protected by scattering and light-reflecting screens 8, was illuminated by ReyLab Xenos RH-1000 luminaries 6 with the power of 1 kW and LED Optronis MultiLED 5 with the luminous flux of 7700 lm. The Screens made it possible to increase the illumination and protect the area of contact of the drop with the liquid from the action of external factors (heating and air flows).

The flow pattern was recorded using Optronis CR3000x2 video camera or Canon EOS350D 2 camera with Canon EFS 18-55 mm lens, which was mounted on a tripod with 5 degrees of freedom. The camcorder or camera is configured by the computer 7.

To enlarge the image, a JJC RR-EOS reversible ring with a diameter of 58 mm and a Canon macro ring with a thickness of 12 mm were used, which enabled to resolve elements with linear dimensions of the order of $10 \mu\text{m}$. The line of sight was $20^\circ\text{--}25^\circ$ or $70^\circ\text{--}75^\circ$ to the horizon, the distance to the drop area was 7–8 cm. A minimum exposure of $1/4000$ s was set for the resolution of reproducible fine-structure components.

The signal to turn on the camera at the selected stage of contact with an adjustable delay was issued by the original control unit 3, which was triggered when a focused drop of the focused laser beam of the chopper 4 intersects.

The control unit is implemented on a microcontroller with a quartz resonator (resonant frequency 16 MHz), tuning accuracy ± 50 Hz. The range of control signal delays varies from $1 \mu\text{s}$ to 10 s. The choice of the delay time made it possible to trace the details of the flow pattern with a small time shift ($\sim 100 \mu\text{s}$) over a wide range of drop heights.

The geometric characteristics of the flow pattern were determined by photometric methods; for scaling, a reference grid with a step of 10 mm was recorded. Data processing was carried out in special programs within the Matlab package.

4 The Geometry of the Flow Formed by a Colored Water Drop Falling into the Water

Starting with the first publications of Worthington [1], the pattern of the splash accompanying the drop falling into the water at rest was photographed from the side or from above and from the side to register the shape of the crown and cumulative jet growth from the water. Increasing the resolution of recording equipment, the brightness of light sources, and changing the position of the line of sight make possible to reveal new details even in a well-studied flow pattern that occurs when a drop of pure water is immersed in still water and the subsequent evolution of characteristic structural elements.

The addition of liquid dyes to the drop fluid (alizarin ink at a concentration of 1:20, Fig. 2) makes it possible to observe in detail the patterns of transfer of droplet material over the deformed surface of the target liquid over a wide time range. An analysis of the early stage of the drop immersion allows us to establish that the bottom of the cavity in the early periods of the drop immersion is flat and in Fig. 2a has a diameter of 0.6 cm. Inclined streamers fly out of the contact area in a wide angular range (from 20° to 50°)—the ejecta sheet is ribbed.

In the phase of the crown development (Fig. 2b), the bottom is already elliptical with axes 0.2 and 0.5 cm. The maximum angle of departure of the jets slightly increases (up to 52°). Separate jets flying from the chevron teeth have a longitudinal size of about 0.22 cm. The chevron edge is uneven, indented. The body of the crown consists of thin vertical painted and unpainted areas, which was described in detail earlier [28].

The zonal structure of the larger ejecting sprays is shown in Fig. 2c (maximum crown height). The diameter of the secondary droplets reaches 0.07. With a complete repeating of the flow basic elements, the flow pattern has a large number of new small elements that reflect the distribution mechanism of the droplet substance. The length of capillary waves moving from the crown chevron varies from 0.071 to 0.058 cm.

The bottom of the cavity is also uneven and contains elements with linear dimensions from 0.043 to 0.33 cm. On the surface of the cavity, the drop material is also unevenly distributed and forms a netlike structure with three and four carbon structures. The number of tiers of the netlike structure and the distribution of droplet matter in it depends on the experimental conditions (in particular, on the We number) [27]. The cellular structures are more expressed during the destruction of the crown (Fig. 2d)—small eddies are recorded at 6 and 9 hours. The number of small vortex structures near the bottom of the cavity is growing rapidly. Larger vortex structures propagate near the surface of the receiving liquid in the direction of the flowing of the crown (in Fig. 2e, left and right). Vortex structures implement the mechanism of transfer of the droplet matter into the target liquid at later phases.

The cumulative jet formed by submerging of an ink drop in water is also colored unevenly. The substance of the drop forms thin filaments—ligaments, the thickness of which varies from 20 to 400 microns. The cumulative jet in Fig. 2f is located on a pedestal with a diameter of 3 cm, inside which the liquid of the drop forms vortex structures. The height of the cumulative jet itself is 3.2 cm. A droplet 0.7 cm in diameter is separated from the top of the cumulative jet (Fig. 2g).

The submerging of a cumulative jet leads to the formation of new vortex processes in the thickness of the liquid. In Fig. 2g to the left of the immersion region, vortices with the step of 0.56, 0.57, and 0.58 cm were identified. The step of the vortex structures on the right is somewhat larger and amounts to 0.65 and 0.79 cm. The new cascade of vortices is caused by the return of a large secondary drop to the target liquid. In Fig. 2h, vortex structures are found to be 0.41 cm wide on the left, 0.47 cm on the bottom for 5 hours, and 0.31 cm and 0.43 cm on the right.

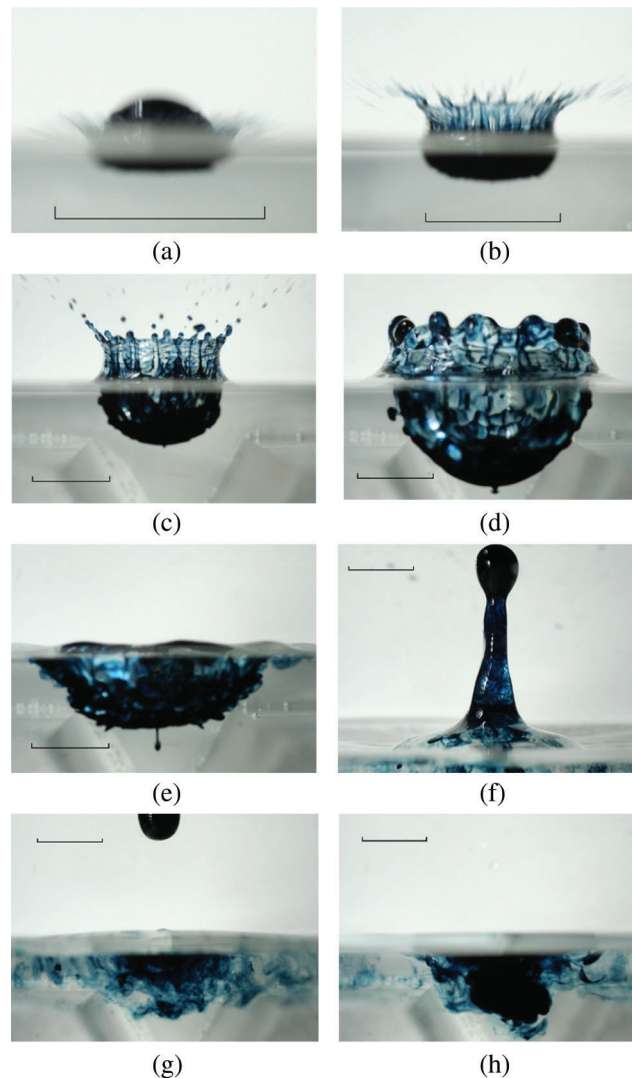


Figure 2: The main stages of the process of submerging an ink drop into the water layer: a) initial contact, b) growing crown with colored ribs, c) the highest crown; d) destruction of the crown, the maximum depth of the cavity, e) ejection of vortex structures from the surface of the cavity, f) highest cumulative jet; g) secondary droplet; h) vortex structures by secondary droplet submerging

The addition of ink to the droplet material makes it possible to identify the fine-structured ruled components—ligaments that appear at the initial stage of drop submerging (upon the destruction of free surfaces) and continue to develop even after the end of all the surface processes. The Line elements have a wide range of spatial scales.

5 Aqueous Solution of Copper Sulfate

In a typical flow pattern with partial submerging of a drop of a saturated solution of copper sulfate (mass fraction 20%, density $\rho = 1.2 \text{ g/cm}^3$) in Fig. 3a, the residual part of the droplet is presented in the center of the concave bottom of the cavity and an expanding veil, separated from the receiving fluid by an annular line. In the direction of 210° and 270° (polar coordinate system) on the surface of a submerging drop, groups of perturbations are visualized, being capillary waves caused by splashes.

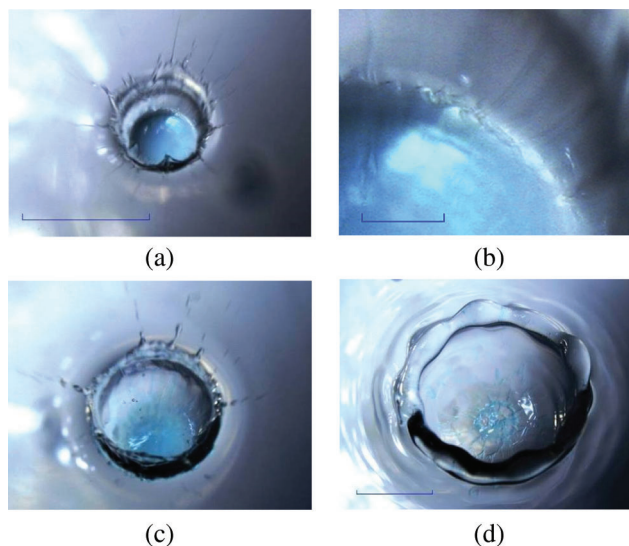


Figure 3: Distribution of a solution of copper sulfate on a perturbed water surface ($H = 80$ cm), marker length on figures a), c), d) is 1 cm; on b) – 0.1 cm

On the enlarged image of the first quarter of the annular cavity (Fig. 3b), periodic structures 0.03–0.05 cm long are observed on the line of contact of the drop with the target liquid. Thin fibrous structures of the contact line are hit into the body of the forming crown. The width of individual fibers is about $2 \cdot 10^{-3}$ cm, which is comparable with the capillary scale for a saturated aqueous solution of other salts.

In the course of time, the walls of the cavity and crown take a cylindrical shape, streamers transform into smoothed teeth. The angle of inclination of the ejecta sheet with a curved outer edge to the horizon increases as the drop submerging. Small fast droplets fly out from the tops of the pointed streamers on the edge of the shroud. Most secondary drops come off the chevron ledges outwards, i.e., in the radial direction from the center of the cavity, however, individual secondary drops with a diameter of 0.08 to 0.2 mm (more than 10 drops here) fly inside the crown (Fig. 3).

The drop material on the inner surface of the crown forms a banded structure with two tiers. The first tier, 0.15 cm long, is adjacent to the edge of the drop residual part, the second, 0.9 cm long, is formed by vertical banded structures.

At the stage of the collapse of the crown, the colored matter is collected in ligaments, which form a complex cellular structure consisting of five tiers with pronounced annular and radial borders at the bottom of the cavity (Fig. 3d). The lower tier is formed by relatively thick fibers (of the order of 0.03 cm); the width of the fibers on the surface of the chevron residue is in the range of 0.005–0.01 cm. In common, the distribution pattern of the droplet material over the deformed surface of the target liquid and the scale of the structures are similar to those considered previously.

6 Acetic Acid Water Solution (9%)

The distribution pattern of a drop of a water solution of acetic acid (9%) has a number of differences from those considered previously. The ejecta sheet formed by submerging of a drop, tinted with blue alizarin ink, is dense and smooth (Fig. 4a). The rest of the droplet is not deformed since it does not get splashes ($R_{\sigma} = 0.14 > 0$).

In course of time, a crown develops, with several banded structures observed on the walls (width of about 0.03 cm), forming a netlike structure with triangular and quadrangular cells (Fig. 4b). However, the

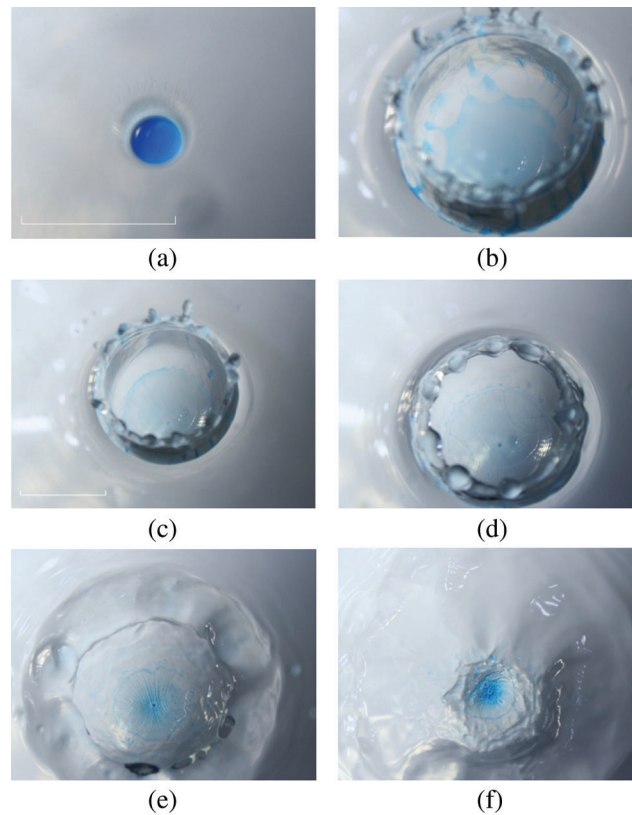


Figure 4: The evolution of flows when a drop of tinted acetic acid (9%) is submerging into clean water ($H = 80$ cm, $D = 0.38$ cm, $h_l = 8$ cm). The length of the marker on [Figs. 5a,c](#) is 1 cm

netlike pattern is irregular, only individual fragments are observed, the number of tiers varies in different directions from the center of the cavity, and later ([Fig. 4c](#)) is replaced by individual fiber structures and an expressed line pattern inside the central spot.

A diffusional colored central spot transforms into a system of arcs (like a saddle) directed to the center of the cavity. The radius of curvature of the arcs increases with approaching to the center of the spot ([Fig. 4d](#)). At distances of 0.04 and 0.16 cm from the system of arcs, ring structures are located that repeat the shape of the painted central region.

In the phase of the collapse of the crown, the colored central region starts to curl up, the ring extending from it collapses, and the concentration of the central spot increases ([Fig. 4e](#)).

The arcs, united by a central spot and an annular boundary, form a grid-ruled structure at the top of a nascent cumulative jet (the inverse picture of the distribution of matter). The matter of the primary droplet is collected at the top of the cumulative jet into a secondary droplet ([Fig. 4f](#)) while maintaining a common line pattern, which scale is commensurate with the scale of the previously considered line structures.

An enlarged image of the distribution pattern of acetic acid is shown in [Fig. 5a](#), where clear concentric arcs with discontinuities limited by a ring structure are presented. In the spatial spectrum of the substance distribution of the drop, a scale of 0.34 cm is distinguished ([Fig. 5b](#)).

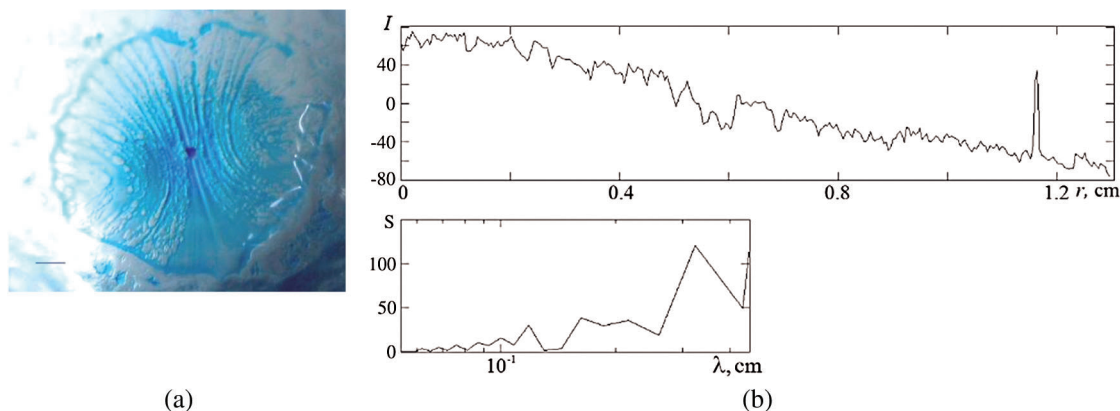


Figure 5: a) The distribution pattern of a drop of acetic acid over the deformed surface of the receiving fluid. Tag size—1 mm. b) Spatial distribution of droplet matter along the axis of concentric arcs (I) and distribution spectrum (S)

7 Submerging of Suspension Drop

At submerging of water drops containing finely dispersed particles of coal (Fig. 6) into clean water, on the inner surface of the crown, the particles form several (from two to four) tiers of a mesh structure (mainly from triangular and quadrangular cells) by analogy with an alizarin ink solution.

At the bottom of the cavity, there is a spot with an almost uniform distribution of particles, on the surface of the crown coal powder builds clear line structures (Fig. 6a). Between the line structures and inside the mesh cells, the powder is practically absent. The height of the tiers of the mesh structure (in Fig. 6a–4 tiers) increases to the crown chevron from 0.08 to 0.3 cm. The suspension distribution on the inner surface of the crown is represented by vertical ruled structures.

As the crown grows (Figs. 6a–d), the cell sizes increase, the cells become more expressed, the boundaries are clear. In Fig. 6b, there are already 6 tiers of netlike structure. In the cells of the lower tier, there is a large number of coal particles. Further, with the destruction of the crown, the distribution of the suspension becomes more expressed annular (Fig. 6d). A protrusion is formed at the bottom of the cavity, containing an accumulation of coal powder. During the formation of a cumulative jet, finely dispersed particles form extended line-loop structures (double looped structure). The main mass of the matter is collected in the center and, further, in the secondary drop at the top of the cumulative stream (Fig. 6f). If the droplet contains larger particles of coal, the netlike structure becomes less expressed, clean areas (not containing powder) become smaller (Fig. 6g). The distribution pattern of coalesced coal clusters forms weakly expressed cells distributed over the entire inner surface of the cavity and crown. The change in the average size of coal particle clusters is shown in Fig. 6h as a function of the distance from the center of the cavity for the flow pattern shown in Fig. 6g.

In general, the distribution of small particles in a suspension quite accurately repeats the distribution of liquid dyes. Significant changes in the distribution pattern are observed in the presence of large clusters with linear dimensions of 0.01–0.09 cm (Fig. 6g).

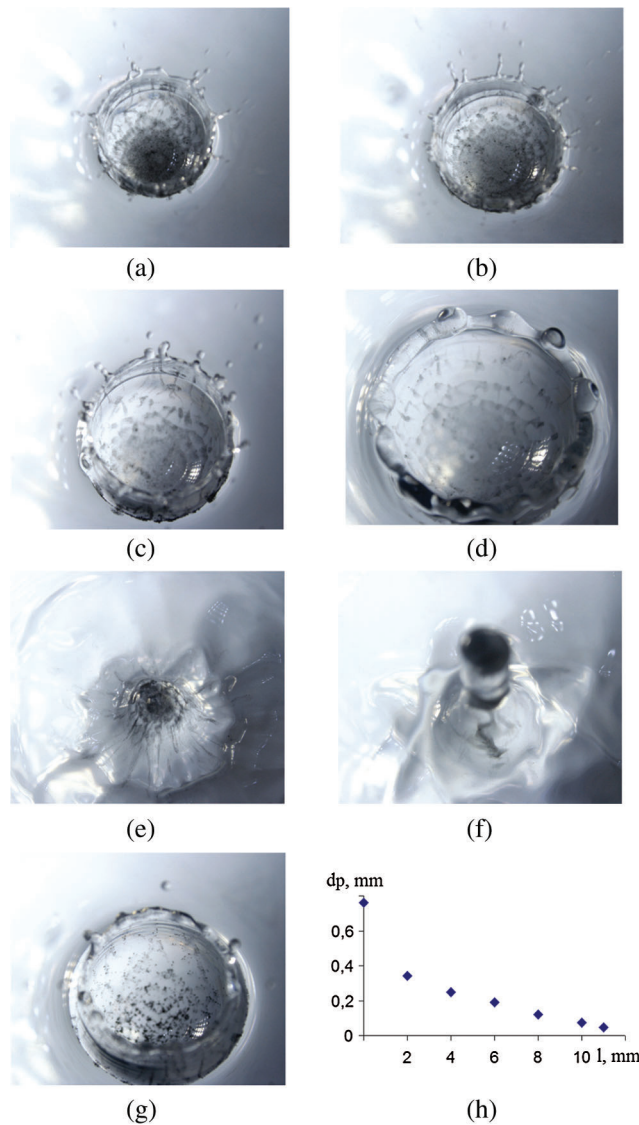


Figure 6: Suspensions splash evolution (coal and size effects). Immersion of a drop of water loaded with coal powder in clean water. Drop height: 80 cm

8 Conclusions

1. The universal flow pattern, which is formed as a result of immersion of a freely falling drop in a liquid, in all the cases includes the following key elements: a primary sheet, a cavity and a crown with capillary waves, a socket (with ribs), a splash and a system of spreading capillary waves.

2. The severity and geometry of the individual elements depend on the physical parameters of the media and the experimental conditions (height and diameter of the droplet).

3. The distribution of large particles of suspensions (clusters) differs from fine particles, which in turn repeat the distribution of liquid dyes.

Acknowledgement: The experiments were performed on the TBP and ESP setups, included in the USF “HPC IPMech RAS.” (2018). Unique Science Facility “Hydrophysical complex for modeling of hydrodynamic processes in the environment and their influence on underwater technical objects, as well as the distribution of impurities in the ocean and atmosphere,” site <http://www.ipmnet.ru/uniquequip/gfk/#equip>.

Funding Statement: This work was supported by the Russian Science Foundation (Project 19-19-00598 “Hydrodynamics and energetics of drops and droplet jets: formation, motion, break-up, interaction with the contact surface,” site: <https://www.rscf.ru/>).

Conflicts of Interest: The author declares that he has no conflicts of interest to report regarding the present study.

References

1. Worthington, A. (1895). *The splash of the drop, series the romance of science*. New York, USA: E. & J.B. Young & Co.
2. Leng, L. (2001). Splash formation by spherical drops. *Journal of Fluid Mechanics*, 427, 73–105. DOI 10.1017/S0022112000002500.
3. Edgerton, H., Killian, J. (1939). *Flash*. Boston: Blanford.
4. Zhang, L., Toole, J., Fezzaa, K., Deegan, R. (2012). Evolution of the ejecta sheet from the impact of a drop with a deep pool. *Journal of Fluid Mechanics*, 690, 5–15. DOI 10.1017/jfm.2011.396.
5. Li, E., Thoraval, M. J., Marston, J., Thoroddsen, S. (2018). Early azimuthal instability during drop impact. *Journal of Fluid Mechanics*, 848, 821–835. DOI 10.1017/jfm.2018.383.
6. Marmanis, H., Thoroddsen, S. (1996). Scaling of the fingering pattern of an impacting drop. *Physics of Fluids*, 8 (6), 1344–1346. DOI 10.1063/1.868941.
7. Thoroddsen, S., Sakakibara, J. (1998). Evolution of the fingering pattern of an impacting drop. *Physics of Fluids*, 10(6), 1359–1374. DOI 10.1063/1.869661.
8. Mundo, C., Sommerfeld, M., Tropea, C. (1995). Droplet-wall collisions: experimental studies of the deformation and breakup process. *International Journal of Multiphase Flow*, 21(2), 151–173. DOI 10.1016/0301-9322(94)00069-V.
9. Cossali, G., Coghe, A., Marengo, M. (1997). The impact of single drop on a wetted solid surface. *Experiments in Fluids*, 22(6), 463–472. DOI 10.1007/s003480050073.
10. Yarin, A., Weiss, D. (1995). Impact of drops on solid surfaces: self-similar capillary waves, and splashing as a new type of kinematic discontinuity. *Journal of Fluid Mechanics*, 283, 141–173. DOI 10.1017/S0022112095002266.
11. Kazachkov, I. (2019). On the modeling of non-classical problems involving liquid jets and films and related heat transfer processes. *Fluid Dynamics & Materials Processing*, 15(5), 491–507. DOI 10.32604/fdmp.2019.06477.
12. Zhang, C., Wu, M. (2019). An analysis of the stretching mechanism of a liquid bridge in typical problems of dip-pen nanolithography by using computational fluid dynamics. *Fluid Dynamics & Materials Processing*, 15(4), 459–469. DOI 10.32604/fdmp.2019.08477.
13. Wang, Z., Dong, K., Zhan, S. (2017). Numerical analysis on unsteady internal flow in an evaporating droplet. *Fluid Dynamics & Materials Processing*, 13(4), 221–234.
14. Chekifi, T., Dennai, B., Khelifaoui, R. (2017). Computational investigation of droplets behaviour inside passive microfluidic oscillator. *Fluid Dynamics & Materials Processing*, 13(3), 173–187.
15. Esmaeeli, A., Behjatian, A. (2017). A note on the transient electrohydrodynamics of a liquid drop. *Fluid Dynamics & Materials Processing*, 13(3), 143–153.
16. Pumphrey, H., Elmore, P. (1990). The entrainment of bubbles by drop impacts. *Journal of Fluid Mechanics*, 220, 539–567. DOI 10.1017/S0022112090003378.
17. Thoroddsen, S. (2002). The ejecta sheet generated by the impact of a drop. *Journal of Fluid Mechanics*, 451, 373–381. DOI 10.1017/S0022112001007030.

18. Yang, X., Kong, S. C. (2019). Adaptive resolution for multiphase smoothed particle hydrodynamics. *Computer Physics Communications*, 239, 112–125. DOI 10.1016/j.cpc.2019.01.002.
19. Thoroddsen, S., Takehara, K., Nguyen, H., Etoh, T. (2018). Singular jets during the collapse of drop-impact craters. *Journal of Fluid Mechanics*, 848(3), 1–14. DOI 10.1017/jfm.2018.435.
20. Chashechkin, Y. D., Ilyinykh, A. (2015). Capillary waves on the surface of the liquid droplets in submerging in a fluid drop. *Doklady Physics*, 60(12), 434–440.
21. Chashechkin, Y. D., Prokhorov, V. (2013). Hydrodynamics of drop impact: short waves on the Crown Surface. *Doklady Physics*, 451, 41.
22. Zhu, G., Li, Z., Fu, D. (2008). Experiments on ring wave packet generated by water drop. *Chinese Science Bulletin*, 53(11), 1634–1638. DOI 10.1007/s11434-008-0468-1.
23. Ray, B., Biswas, G., Sharma, A. (2015). Regimes during liquid drop impact on a liquid pool. *Journal of Fluid Mechanics*, 768, 492–523. DOI 10.1017/jfm.2015.108.
24. Perryman, S., Clark, S., West, J. (2015). Splash dispersal of *Phyllosticta citricarpa* conidia from infected citrus fruit. *Scientific Reports*, 4(6568), 1–8. DOI 10.1038/srep06568.
25. Kondo, T., Ando, K. (2019). Simulation of high-speed droplet impact against a dry/wet rigid wall for understanding the mechanism of liquid jet cleaning. *Physics of Fluids*, 31(1), 013303. DOI 10.1063/1.5079282.
26. Mitrias, C., Jaensson, N., Hulsen, M., Anderson, P. (2019). Head-on collision of Newtonian drops in a viscoelastic medium. *Microfluidics and Nanofluidics*, 23(7), 199. DOI 10.1007/s10404-019-2254-6.
27. Chashechkin, Y. D., Ilyinykh, A. Y. (2018). Banded structures in the distribution pattern of a drop over the surface of the target fluid. *Doklady Physics*, 63(7), 282–287. DOI 10.1134/S1028335818070066.
28. Chashechkin, Y. D., Prokhorov, V. E. (2016). Transformation of the bridge during drop separation. *Journal of Applied Mechanics and Technical Physics*, 57(3), 402–415. DOI 10.1134/S0021894416030032.